IEEE Access
Multidisciplinary | Rapid Review | Open Access Journal

Received March 21, 2019, accepted March 29, 2019, date of publication April 3, 2019, date of current version April 18, 2019.

Digital Object Identifier 10.1109/ACCESS.2019.2909056

Energy Consumption Minimizing for Electro-Hydraulic Servo Driving Planar Parallel Mechanism by Optimizing the Structure Based on Genetic Algorithm

JINSONG ZHAO[1,2,3,5], TAO YANG[3], ZHILEI MA[3], CHIFU YANG[4], ZHIPENG WANG[3], AND CHUNFA WANG[3]

[1]Hebei Provincial Key Laboratory of Heavy Machinery Fluid Power Transmission and Control, Yanshan University, Qinhuangdao 066004, China
[2]Key Laboratory of Advanced Forging & Stamping Technology and Science (Yanshan University), Ministry of Education of China, Qinhuangdao 066004, China
[3]School of Mechanical Engineering, Yanshan University, Qinhuangdao 066004, China
[4]State Key Laboratory of Robotics and System of China, Harbin Institute of Technology, Harbin 150001, China
[5]State Key Laboratory of Fluid Power and Mechatronic Systems, Zhejiang University, Hangzhou 310013, China

Corresponding author: Chifu Yang (wzpysu@163.com)

This work was supported in part by the National Natural Science Foundation of China under Grant 51505412 and Grant 51575471, and in part by the Open Foundation of the State Key Laboratory of Fluid Power and Mechatronic Systems under Grant GZKF-201807.

ABSTRACT Electro-hydraulic servo driving planar parallel mechanism (EHPM) is widely used in simulating large-scale vibration environments. However, the energy consumption of EHPM is large. There is little research on the energy consumption of EHPM. Therefore, this paper presents a structural optimization method, which can effectively reduce the energy consumption of EHPM by changing the arrangement of the planar redundant actuator. First, the mathematical model of the total power of EHPM is established. In order to distinguish the variables that affect energy consumption, the effect of a single structural variable on energy consumption is discussed, respectively, based on the mathematical model of the total power. And then the genetic algorithm is used to optimize the total power objective function with multiple structural variables. The influence of the initial value of the structure variable on the convergence range of total power is also discussed. The simulation results show the effectiveness of changing the actuator arrangement, which can significantly reduce energy consumption. Moreover, the component selecting of the hydraulic cylinder and servo valve can be smaller and the cost of which can be reduced.

INDEX TERMS Electro-hydraulic servo, energy consumption, genetic algorithm, planar parallel mechanism, structure optimization.

I. INTRODUCTION

The parallel mechanism has the advantages of strong bearing capacity, small inertia, fast movement and so on. Currently the parallel mechanism is widely used in seismic environment simulation [1], flight simulator [2], parallel machine tool [3] and other aspects. Specially, it has a great advantage in a large motion environment simulation. However, EHPM is less efficient. The power loss is very large in large-scale simulation environment, which not only wastes energy but also increases the cost of hydraulic components. Therefore, it is of great significance to reduce the energy consumption of EHPM.

At present, research on reducing energy consumption and improving efficiency mainly focuses on equipment such as robots [4], [5], exoskeletons [6], and prostheses [7]. Since the power source of the robot itself is limited, the method of reducing energy consumption and improving efficiency can effectively solve the problem of battery life. Some scholars have optimized the design from the aspect of stiffness [8], [9]. Ackerman and Seipel [10] proposed to apply the elastic load suspension mechanism to a hexapod robot. The experiment shows that the robot with elastic load suspension mechanism consumed up to 24% less power than with

The associate editor coordinating the review of this manuscript and approving it for publication was Jianyong Yao.

a rigidly attached load. Bauer *et al.* [11], [12] proposed elastic couplings mechanical springs to optimize the energy efficiency of walking bipedal robots by more than 80 % in a speed range from 0.3 to 2.3m/s. In the study of energy consumption of quadruped robots [13], the reasonable gait parameters are determined to reduce energy consumption significantly. In [14], a new design is presented for a 3 degree of freedom (DOF) leg based on gravity decoupling. Energy-efficient configurations [15] was discussed by comparing insect and mammal on the hexapod robotic platform SILO6. The experiment results that power consumption of insect configuration exceeds that of mammal configuration during crab walking. Phan *et al.* [16] proposed a control method of look-up table for flexible manipulators to reduce energy consumption. The objective function of energy consumption is minimized by optimizing the positive position feedback parameters. The torque distribution algorithm [17] is designed to reduce energy consumption in order to meet the energy requirements of legged robots.

However, the research on electro-hydraulic servo parallel mechanisms has focused on improving the dynamic tracking performance through controller design [18]–[20] and improving the working range through structural design [21], [22]. For example, an advanced nonlinear controller for hydraulic system was developed in [20] to achieve asymptotic tracking with various disturbances. From the perspective of hydraulic system design, for servo control systems with small power, fast response and high precision, servo valve control systems [23] are mostly used. Servo pump control systems [24] are used in high-power electro-hydraulic servo systems to reduce energy consumption. And usually in the design of the hydraulic system, the use of accumulators [25], [26] for energy recovery and reuse has achieved the goal of reducing energy consumption and improving efficiency. Hydraulic system design is just some of the most basic methods, and the actual reduction of energy loss over a large scale still needs further study. Some scholars reduce power loss by using controller design and other advanced algorithms. Braune *et al.* [27] presented a control strategy based on a nonlinear model for an electromagnetic valve actuator in order to meet the requirement of low power consumption, and energy consumption is reduced remarkably. Mohammad *et al.* [28] designed sliding-mode control with a nonlinear sliding surface for machine tools, through which consumed energy was reduced by about 12.9%. Uchiyama *et al.* [29] proposed a novel controller based on a contouring control in order to reduce energy consumption in five-axis machine tools. The experiment results show that the energy consumption reduced by 4%. An efficient online trajectory planning algorithm [30] was proposed for a straight-line path for three-wheeled omnidirectional mobile robots. And experiment results show that these minimum-energy trajectories can save energy up to 4.76%. Some scholars use structural optimization to reduce power loss. Wu *et al.* [31] proposed a novel U-3PSS two-axis sun-tracking mechanism with parallel mechanism. The results show that the novel U-3PSS solar tracker has a smaller energy consumption compared with U-2PSS solar tracker. Yao *et al.* [32] presented that the redundant actuation could reduce the energy consumption of the parallel mechanism. Experimental results show that redundant actuation can reduce energy consumption by up to 45% compared to the nonredundant actuation. Bidgoly *et al.* [33] proposed to combine the structure design of kinematic redundancy and multi objective optimization method, which effectively reduced energy consumption. Plooij *et al.* [34] used the bidirectional clutched parallel elastic actuator to reduce the energy consumption of robots. Simulations show that the energy consumption can be reduced 73%. These documents illustrate the effectiveness of reducing energy losses through structural optimization. However, there is not research on the structure optimization through the arrangement of actuators and the distribution of hinges, which can be seen as a problem of finding the optimal solution in multiple variables. There are many advanced algorithms for multivariable optimal control, such as genetic algorithms (GA) [35], [36] and other real-time algorithms [37], [38].

The main contribution this paper is to propose a new structural optimization method, for EHPM. It reduces the energy consumption of EHPM by changing the arrangement of the planar redundant actuator. In order to distinguish the variables that affect energy consumption, the effect of a single structural variable on energy consumption is discussed respectively. GA is used to optimize the total power objective function with multiple structural variables. And the influence of the initial value of the structure variable on the convergence range of total power is also discussed. Finally, it reduces the maximum flow of the single hydraulic cylinder and the average flow of EHPM during the working process. The significant meaning is that the cost and energy consumption of EHPM are reduced effectively.

This paper is organized as following. Section 2 presents the kinematic model of EHPM. Section 3 establishes the mathematical model of the total power of EHPM. The total power mathematical modeling of EHPM is optimized based on GA in Section 4. And the optimum parameters that affect the total power of EHPM are obtained. In Section 5, we analyze and evaluate the optimal design results, which verifies the validity of the experiment. Finally, main conclusions are summarized in Section 6.

II. THE KINEMATIC MODELING

Classic shaker structure is shown in Fig. 1. The EHPM is shown in Fig. 2. The coordinate system of the EHPM is shown as Fig. 3. $O - X_O Y_O Z_O$ is the inertial coordinate system. $O_P - X_P Y_P Z_P$ is the follow-up coordinate system, which is fixed to the EHPM. The two coordinate systems are coincident when the EHPM is in the initial position.

In Fig. 3, $\mathbf{a}_i$ $(i = 1, 2, 3, 4)$ is the coordinate vector of the upper hinge points on the EHPM, $\mathbf{b}_i$ $(i = 1, 2, 3, 4)$ is the coordinate vector of the lower hinge points on the EHPM.

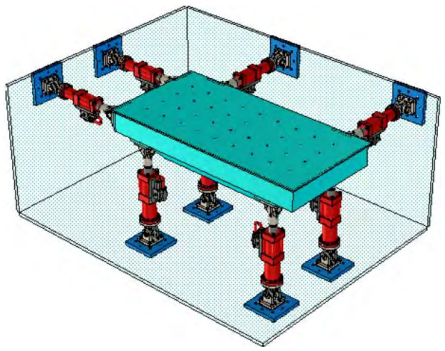

FIGURE 1. The structure of the classical shaking table.

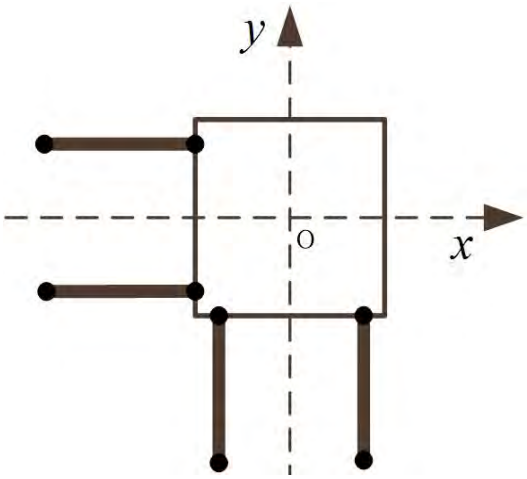

FIGURE 2. The structure of the EHPM.

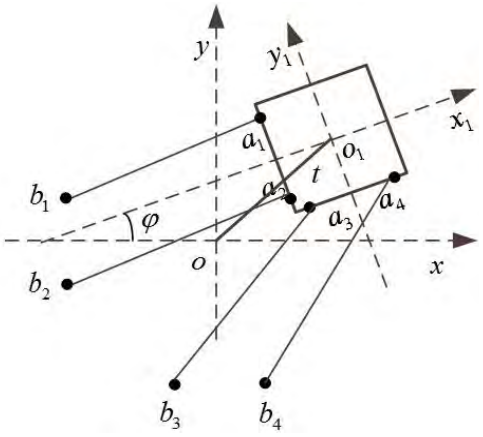

FIGURE 3. Coordinate system description of the EHPM.

The generalized pose of the follow-up coordinate system relative to the inertial coordinate system is defined as

$$\mathbf{q} = \begin{bmatrix} q_1 & q_2 & q_3 \end{bmatrix}^T \tag{1}$$

where q_1 is the displacement of the EHPM along the x coordinate system. q_2 is the displacement of the EHPM along the y coordinate system, q_3 is the angle that follow-up coordinate system rotates counterclockwise relative to the inertial coordinate system.

The rotation transformation matrix of the follow-up coordinate system relative to the inertial coordinate system can be expressed as

$$\mathbf{R} = \begin{bmatrix} \cos q_3 & -\sin q_3 \\ \sin q_3 & \cos q_3 \end{bmatrix} \tag{2}$$

$$\mathbf{R} = \mathbf{R}'\omega \tag{3}$$

where ω is the angular velocity of the platform.

Hydraulic cylinder length vector can be obtained as

$$\mathbf{l_i} = \mathbf{t} + \mathbf{R}\mathrm{a}_i - \mathbf{b}_i, (i = 1, 2, 3, 4) \tag{4}$$

where $t = \begin{bmatrix} q_1 & q_2 \end{bmatrix}^T$

The length of the hydraulic cylinder can be expressed as

$$l_i = \sqrt{(\mathbf{t} + \mathbf{R}\mathrm{a}_i - \mathbf{b}_i)^T(\mathbf{t} + \mathbf{R}\mathrm{a}_i - \mathbf{b}_i)}\ (i = 1, 2, 3, 4) \tag{5}$$

The length of the hydraulic cylinder is set to l_0 when the EHPM is in the initial position. And then the displacement change of the hydraulic cylinder can be obtained as

$$\Delta l_i = l_i - l_0, (i = 1, 2, 3, 4) \tag{6}$$

By combining (5) with (6), (7) can be obtained as

$$(\Delta l_i + l_0)^2 = \sum_{j=1}^{2} \left(\mathbf{q}_j + (\mathbf{R}\mathrm{a}_i)_j - \mathbf{b}_{ij}\right)^2 \tag{7}$$

Equation (7) can be rewritten as

$$f\ (q_1, q_2, q_3) = \sum_{j=1}^{2} \left(\mathbf{q}_j + (\mathbf{R}\mathrm{a}_i)_j - \mathbf{b}_{ij}\right)^2 - (\Delta l_i + l_0)^2 = 0 \tag{8}$$

The function $f\ (q_1, q_2, q_3)$ is expanded using the Taylor formula in the $Q_0 = (q_{10}, q_{20}, q_{30})$. Round off the high-order differential terms, the following linear equations can be obtained as

$$\begin{cases} f_1\ (Q_0) + \sum_{i=1}^{3} (q_i - q_{i0}) \dfrac{\partial f_1\ (Q_0)}{\partial q_i} = 0 \\ f_2\ (Q_0) + \sum_{i=1}^{3} (q_i - q_{i0}) \dfrac{\partial f_2\ (Q_0)}{\partial q_i} = 0 \\ f_3\ (Q_0) + \sum_{i=1}^{3} (q_i - q_{i0}) \dfrac{\partial f_3\ (Q_0)}{\partial q_i} = 0 \\ f_4\ (Q_0) + \sum_{i=1}^{3} (q_i - q_{i0}) \dfrac{\partial f_4\ (Q_0)}{\partial q_i} = 0 \end{cases} \tag{9}$$

Define $\Delta q_i = q_i - q_{i0}\ (i = 1, 2, 3)$. Equation (9) can be regarded as a linear system of equations with variable Δq_i as unknown. Coefficient matrix can be expressed as

$$\mathbf{J} = \begin{bmatrix} \dfrac{\partial f_1}{\partial q_1} & \dfrac{\partial f_1}{\partial q_2} & \dfrac{\partial f_1}{\partial q_3} \\ \dfrac{\partial f_2}{\partial q_1} & \dfrac{\partial f_2}{\partial q_2} & \dfrac{\partial f_2}{\partial q_3} \\ \dfrac{\partial f_3}{\partial q_1} & \dfrac{\partial f_3}{\partial q_2} & \dfrac{\partial f_3}{\partial q_3} \\ \dfrac{\partial f_4}{\partial q_1} & \dfrac{\partial f_4}{\partial q_2} & \dfrac{\partial f_4}{\partial q_3} \end{bmatrix} \tag{10}$$

Equation (9) can be rewritten as $\mathbf{J}\Delta\mathbf{q} = -\mathbf{f}(Q_0)$. And the iterative recursion formula can be obtained as $\mathbf{J}(\mathbf{q}_{k+1} - \mathbf{q}_k) = -\mathbf{f}(Q_k)$. The following transformation needs to be done in order to avoid pseudo-inverse

$$\mathbf{J}^T\mathbf{J}(\mathbf{q}_{k+1} - \mathbf{q}_k) = -\mathbf{J}^T\mathbf{f}(Q_k) \tag{11}$$

If $\mathbf{J}^T\mathbf{J}$ is not singular, the recurrence formula is

$$\mathbf{q}_{k+1} = -\left(\mathbf{J}^T\mathbf{J}\right)^{-1}\mathbf{J}^T f(Q_k) + \mathbf{q}_k \tag{12}$$

By deriving on both sides of the (5), (13) can be obtained as

$$\dot{l}_i = \frac{(t + \mathbf{R}a_i - b_i)^T}{|l_i|}\left(\dot{\mathbf{t}} + \mathbf{R}'\mathrm{a}_i\right) = \mathbf{l}_{ni}^T\left(\mathbf{t} + \mathbf{R}'\mathrm{a}_i\right) \tag{13}$$

where $\mathbf{l}_{ni}$ is the unit direction vector for the direction of the leg.

By substituting (3) to (13), (13) can be rewritten as

$$\dot{l}_i = \mathbf{l}_{ni}^T\dot{\mathbf{t}} + \mathbf{l}_{ni}^T\mathbf{R}'\mathrm{a}_i\dot{\phi} = \left(\mathbf{l}_{ni}^T + \mathbf{l}_{ni}^T\mathbf{R}'\mathrm{a}_i\right)\left[\dot{x}, \dot{y}, \dot{\phi}\right]^T \tag{14}$$

$$\dot{\mathbf{l}} = \mathbf{J}_{lq}\dot{\mathbf{q}} \tag{15}$$

The Jacobian matrix is

$$\mathbf{J}_{lq} = \begin{bmatrix} \mathbf{l}_{n1}^T & \mathbf{l}_{n1}^T\mathbf{R}'\mathrm{a}_1 \\ \mathbf{l}_{n2}^T & \mathbf{l}_{n2}^T\mathbf{R}'\mathrm{a}_2 \\ \mathbf{l}_{n3}^T & \mathbf{l}_{n3}^T\mathbf{R}'\mathrm{a}_3 \\ \mathbf{l}_{n4}^T & \mathbf{l}_{n4}^T\mathbf{R}'\mathrm{a}_4 \end{bmatrix} \tag{16}$$

III. MATHEMATICAL MODELING OF TOTAL POWER FOR EHPM

A. OPTIMIZATION HYPOTHESIS

The EHPM can be optimized by changing the layout of the actuator and the location of the upper and lower hinge points. For the square platform mechanism, the following assumptions are made. The upper hinge point of the EHPM is evenly distributed on one circle. The lower hinge point of the EHPM is evenly distributed on one circle. The two distribution circles are concentric, and the distribution radius of lower hinge point is greater than the upper hinge point. The upper and lower hinge points are sequentially connected to form a EHPM.

B. MATHEMATICAL MODELING OF TOTAL POWER OF EHPM

The schematic diagram of EHPM optimization is shown in Fig. 4. $\mathbf{a}_i$ $(i = 1, 2, 3, 4)$ is upper hinge point, and $\mathbf{b}_j$ $(j = 1, 2, 3, 4)$ is lower hinge point. Assuming the distribution radius of the upper hinge pointer is r_1. The angle between the positive x-axis and the radius located by $\mathbf{a}_1$ is α. When the EHPM is in the initial position, the angle between the hydraulic cylinder and the positive x-axis is θ. The structure of EHPM depends on r_1, α, θ, and l_0. Therefore, r_1, α, θ, and l_0 are initially selected as structural optimization variables.

The coordinate matrix of the upper hinge is

$$\mathbf{A} = \begin{bmatrix} r_1\cos\alpha & -r_1\sin\alpha & -r_1\cos\alpha & r_1\sin\alpha \\ r_1\sin\alpha & r_1\cos\alpha & -r_1\sin\alpha & -r_1\cos\alpha \end{bmatrix} \tag{17}$$

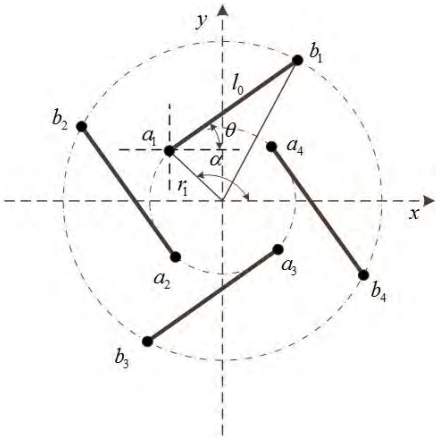

FIGURE 4. Schematic diagram of EHPM optimization.

The coordinate matrix of the lower hinge is

$$\mathbf{B} = \begin{bmatrix} l_0\cos\theta + r_1\cos\alpha & l_0\sin\theta + r_1\sin\alpha \\ -l_0\sin\theta - r_1\sin\alpha & l_0\cos\theta + r_1\cos\alpha \\ -l_0\cos\theta - r_1\cos\alpha & -l_0\sin\theta - r_1\sin\alpha \\ l_0\sin\theta + r_1\sin\alpha & -l_0\cos\theta - r_1\cos\alpha \end{bmatrix}^T \tag{18}$$

According to the known maximum output force $F_{\max}$ and maximum speed $v_{\max}$ of EHPM, the effective working area and the maximum flow of the hydraulic cylinder are calculated. In order to establish the mathematical model of the total power of EHPM, it is necessary to establish the force transformation relationship from the DOF space to the joint space, the equation of which can be expressed as

$$\mathbf{F}^T\delta\mathbf{q} = \mathbf{f}_a^T\delta\mathbf{l} \tag{19}$$

where $\mathbf{F}$ is generalized force acting on EHPM, $\mathbf{f}_a$ is output force of hydraulic cylinder.

By substituting (15) into (19), the relationship between $\mathbf{F}$ and $\mathbf{f}_a$ can be obtained as

$$\mathbf{f}_a = \left(\mathbf{J}_{lq}^T\right)^{-1}\mathbf{F} \tag{20}$$

When the output of the generalized force is maximum, the maximum output force of the hydraulic cylinder can be calculated as

$$\mathbf{f}_{a\max} = \left(\mathbf{J}_{lq}^T\right)^{-1}\mathbf{F}_{\max} \tag{21}$$

According to the principle of load matching, the effective action area of hydraulic cylinder is designed as

$$A = \frac{3}{2}\frac{f_{a\max}}{P_s} \tag{22}$$

where P_s is the oil supply pressure.

The maximum functional curve of the EHPM is shown in Fig. 5. In the case of $\omega = \omega_3$, the maximum velocity and the maximum acceleration occur simultaneously. Therefore, the condition $\omega = \omega_3$ is taken as the basis for modeling.

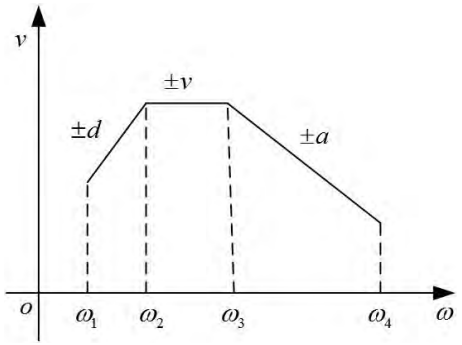

FIGURE 5. Maximum function curve shaking table.

The displacement command of the EHPM is set to $d = A_d \sin(\omega t + \phi)$, and then the speed and acceleration commands of the EHPM can be obtained as $v = A_d\omega \cos(\omega t + \phi)$, $a = -A_d\omega^2 \sin(\omega t + \phi)$, respectively.

When the maximum speed and maximum acceleration occur simultaneously, the displacement command of the EHPM can be expressed as

$$d = \frac{v_{\max}^2}{a_{\max}} \sin\left(\frac{a_{\max}}{v_{\max}} t\right) \tag{23}$$

The research object of this article is the shaking table, which is mainly used in vehicle road simulation and seismic environment simulation. Under this condition, the tested object and the upper platform are in a fixed state. Besides, the optimization shaking table is planar parallel mechanism, so the effect of gravity can be neglected. In this study, the vibration frequency of shaking table is very high, and thus inertial force is the main factor affecting energy consumption. Therefore, this study only considers the influence of inertial force on structure optimization and ignore other interferences.

Under special external disturbance, the corresponding energy consumption model can be established, which is similar to the energy consumption model of inertial force. And then the total energy consumption is taken as the optimization objective, and the presented method based on GA still works for optimization.

When the EHPM moves in the x-axis direction according to the (23), the generalized pose and generalized velocity can be obtained respectively as

$$\mathbf{q}(t) = \begin{bmatrix} \frac{v_{\max}^2}{a_{\max}} \sin\left(\frac{a_{\max}}{v_{\max}} t\right) & 0 & 0 \end{bmatrix}^T \tag{24}$$

$$\dot{\mathbf{q}}(t) = \begin{bmatrix} v_{\max} \cos\left(\frac{a_{\max}}{v_{\max}} t\right) & 0 & 0 \end{bmatrix}^T \tag{25}$$

Similarly, the generalized poses and generalized velocities along other DOFs can also be obtained. The total flow of the four hydraulic cylinders is

$$Q(t) = A \sum_{i=1}^{4} \left|\dot{l}_i(t)\right| \tag{26}$$

TABLE 1. Kinematic index of EHPM.

	Maximum Displacement	Maximum speed	Maximum acceleration
X axis	±0.5m	±10m/s	±20.0g
Y axis	±0.5m	±10m/s	±20.0g
Spin	±15°	±50°/s	±250°/s^2

According to (26), the total power of EHPM in the time T range can be obtained as

$$P = P_s \frac{A}{T} \int_0^T \left(\sum_{i=1}^{4} \left|\dot{l}_i(t)\right|\right) dt \tag{27}$$

IV. OPTIMIZATION DESIGN AND ANALYSIS BASED ON GA

A. THE INFLUENCE OF UNIVARIATE ON THE TOTAL POWER OF EHPM

Although r_1, α, l_0, θ can determine the structure of the EHPM, the impact of each variable on energy consumption needs further study. Therefore, the effect of each structural variable needs to be test respectively on the total power of EHPM, thereby determining valid optimization variables.

Table 1 is the kinematic parameters of EHPM. The minimum size of the platform be a square with a side length of one. The quality of EHPM is 630kg, and the pressure of the hydraulic drive system is 18Mpa. When the maximum speed of the platform and the maximum acceleration occur simultaneously, the displacement command of the EHPM is $d(t) = 0.45 \sin(20.0t)$. The speed and acceleration commands of the EHPM are $v(t) = 9.0 \cos(20.0t)$ and $a(t) = -180.0 \sin(20.0t)$ respectively. The rotation command of the EHPM is $\phi(t) = 10 \sin(5.0t)$. Under the above conditions, the sum of the total power can be calculated. In this process, first of all, set initial values for variables to be optimized and calculate the coordinates of hinge to determine the effective working area of hydraulic cylinder. The specific method is to divide the workspace into several coordinate points by the step size of 1mm on the coordinate axis, and calculate the corresponding hydraulic cylinder area according to each divided coordinate points based on the principle of best load matching. And then, select the maximum value among them as the effective working area of hydraulic cylinder. Finally, under the condition that the maximum velocity and acceleration occur simultaneously, the average total flow rate of the hydraulic driven system can be calculated, and further the total power is calculated. The program flow diagram of total power modeling process for EHPM is shown in Fig. 6, and the feedback in which just play an exhaustive role to find out the maximum hydraulic cylinder area in the whole work space.

The mechanical interference and other constraints are not considered at first. Therefore, the effect of a single variable on the total power of EHPM is discussed only from a mathematical perspective. Firstly, a series of discrete values of the test variable is given. And then the upper and lower bounds

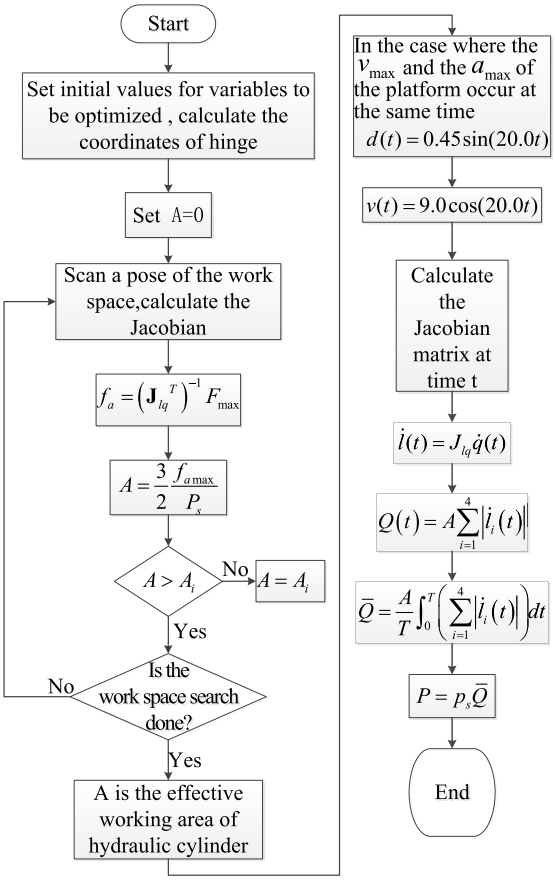

FIGURE 6. The program flow diagram of total power modeling process.

TABLE 2. Effect of θ on total power.

Decision variables	Unit	Value
θ	rad	$0 \le \theta \le 2\pi$
Constraints	Unit	Value
r_1	m	$0.5 \le r_1 \le 1.5$
α	rad	$0 \le \alpha \le 2\pi$
l_0	m	$2 \le l_0 \le 3.4$
Objectives	Unit	Value
P	kW	Cyclical changes

of other variables are limited. Finally, the curve of minimum total power that can reflect the change of the minimum total power with the change of test variable can be obtained.

Set the step size of θ be 5°, which changes from 0° to 360°. The boundary constraint of optimized variables is $\left[\begin{array}{ccc} 0.5 & 0 & 2 \end{array}\right] \le \left[\begin{array}{ccc} r_1 & \alpha & l_0 \end{array}\right] \le \left[\begin{array}{ccc} 1.5 & 2\pi & 3.4 \end{array}\right]$. The data is shown in Table 2. The total power variation curve affected by the variable θ is shown in Fig. 7.

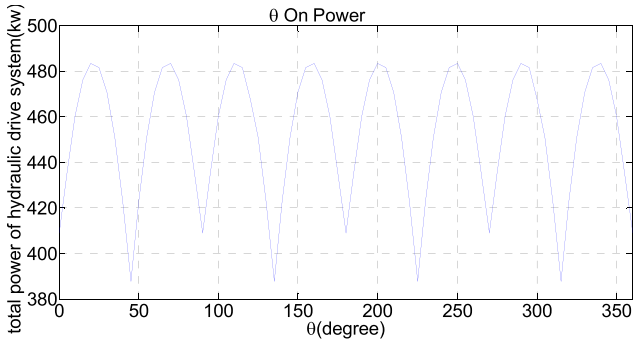

FIGURE 7. Effect of θ on total power.

TABLE 3. Effect of α on total power.

Decision variables	Unit	Value
α	rad	$0 \le \alpha \le 2\pi$
Constraints	Unit	Value
r_1	m	$0.5 \le r_1 \le 1.5$
θ	rad	$0 \le \theta \le 2\pi$
l_0	m	$2 \le l_0 \le 3.4$
Objectives	Unit	Value
P	kW	Fixed value

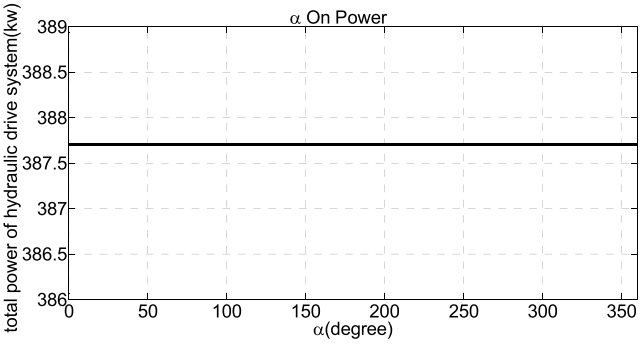

FIGURE 8. Effect of α on total power.

From Fig. 7, it can be seen that the total power changes periodically following increase of θ, and the minimum of the total power locates at the angles of $45° + \lambda \cdot 90°$ ($\lambda \in Z$). Set the step size of α be 5°, which changes from 0° to 360°. The boundary constraint of optimized variables is $\left[\begin{array}{ccc} 0.5 & 0 & 2 \end{array}\right] \le \left[\begin{array}{ccc} r_1 & \theta & l_0 \end{array}\right] \le \left[\begin{array}{ccc} 1.5 & 2\pi & 3.4 \end{array}\right]$. The data is shown in Table 3. The total power variation curve affected by the variable α is shown in Fig. 8. Set the step size of l_0 be 0.1m, which changes from 2m to 3.4m. The boundary constraint of optimized variables is $\left[\begin{array}{ccc} 0.5 & 0 & 0 \end{array}\right] \le \left[\begin{array}{ccc} r_1 & \theta & \alpha \end{array}\right] \le \left[\begin{array}{ccc} 1.5 & 2\pi & 2\pi \end{array}\right]$. The data is shown in Table 4. The total power variation curve

TABLE 4. Effect of l_0 on total power.

Decision variables	Unit	Value
l_0	m	$2 \le l_0 \le 3.4$
Constraints	Unit	Value
r_1	m	$0.5 \le r_1 \le 1.5$
θ	rad	$0 \le \theta \le 2\pi$
α	rad	$0 \le \alpha \le 2\pi$
Objectives	Unit	Value
P	kW	Monotone decreasing

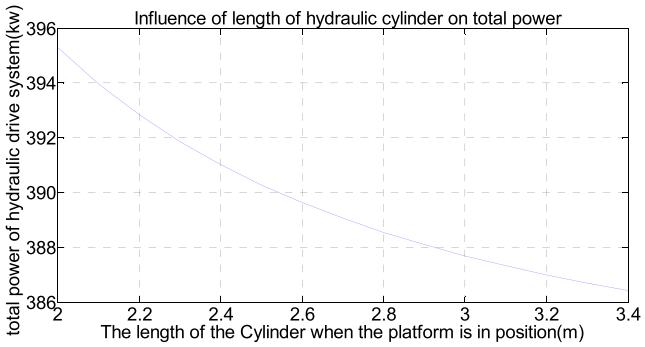

FIGURE 9. Effect of l_0 on total power.

TABLE 5. Effect of r_1 on total power.

Decision variables	Unit	Value
r_1	m	$0.5 \le r_1 \le 1.5$
Constraints	Unit	Value
l_0	m	$2 \le l_0 \le 3.4$
θ	rad	$0 \le \alpha \le 2\pi$
α	rad	$0 \le \alpha \le 2\pi$
Objectives	Unit	Value
P	kW	Fixed value

affected by the variable l_0 is shown in Fig. 9. Set the step size of r_1 be 0.05m, which changes from 0.5m to 1.5m.The boundary constraint of optimized variables is $\begin{bmatrix} 2 & 0 & 0 \end{bmatrix} \le \begin{bmatrix} l_0 & \theta & \alpha \end{bmatrix} \le \begin{bmatrix} 3.4 & 2\pi & 2\pi \end{bmatrix}$. The data is shown in Table 5. The total power variation curve affected by the variable r_1 is shown in Fig. 10.

It can be seen that θ has a significant effect on the total power. The total power reaches minimum and the

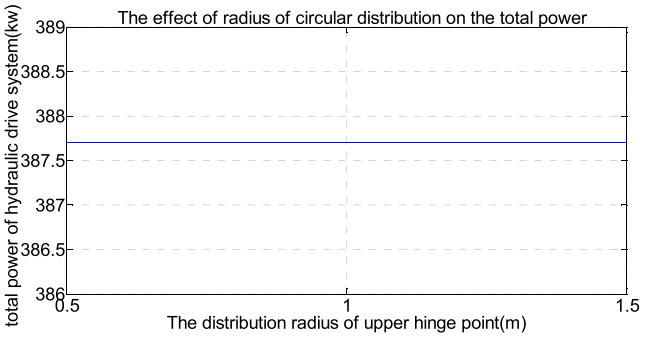

FIGURE 10. Effect of r_1 on total power.

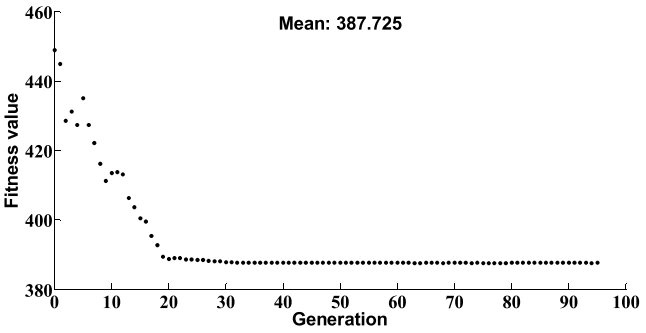

FIGURE 11. Results of GA.

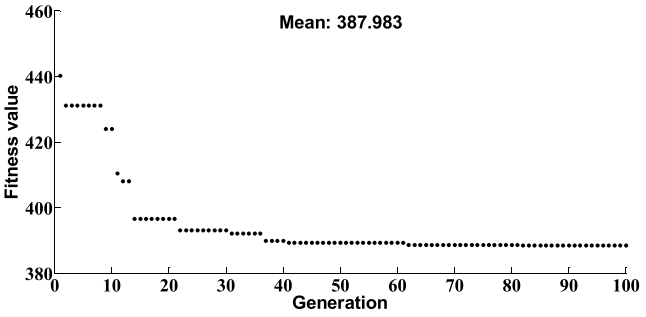

FIGURE 12. Results of PSO algorithm.

corresponding values are equal when $\theta = 45°$, $\theta = 135°$, $\theta = 225°$, $\theta = 315°$. The curve shows a periodic change with a period of 90°. As the length of the hydraulic cylinder grows, the total power monotonically decreases. With the change of α and r_1, the total power does not change. So α and r_1 are no longer optimization variables. Taking into account the compact structure, $r_1 = 1.061$m, $\alpha = 120°$ and the boundary condition of $X = \begin{bmatrix} l_0 & \theta \end{bmatrix}$ is $\begin{bmatrix} 2.525 & 0 \end{bmatrix} \le X \le \begin{bmatrix} 3 & 2\pi \end{bmatrix}$

B. OPTIMIZATION DESIGN BASED ON GA

The optimization problem is to search out a set of solutions from the variables under certain constraints so that the objective function takes the minimum. In this paper, the objective function is the total power mathematical model of EHPM. The objective function has two optimization variables.

TABLE 6. The values of the tuning parameters of the GA.

	Tuning parameters	Value
population	population size	20
reproduction	elite count	1
	crossover fraction	0.8
migration	direction	forward
	fraction	0.2
	interval	20
constraint parameters	initial penalty	10
	penalty factor	100
stopping criteria	function tolerance	10^{-5}
	constraint tolerance	10^{-5}

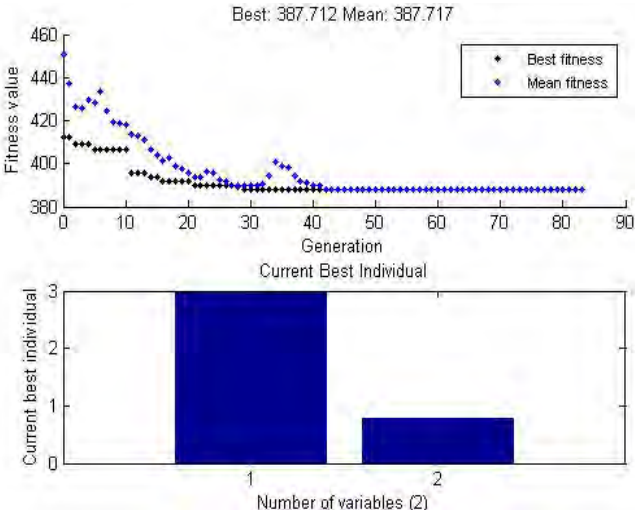

FIGURE 13. The result when the initial value is [0; 1].

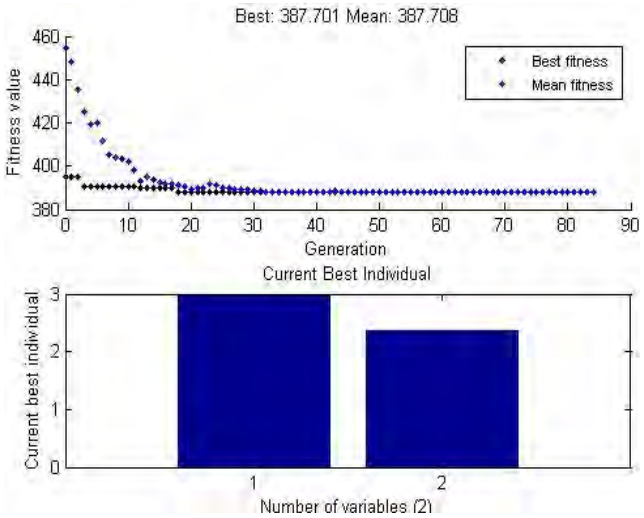

FIGURE 14. The result when the initial value is [1; π].

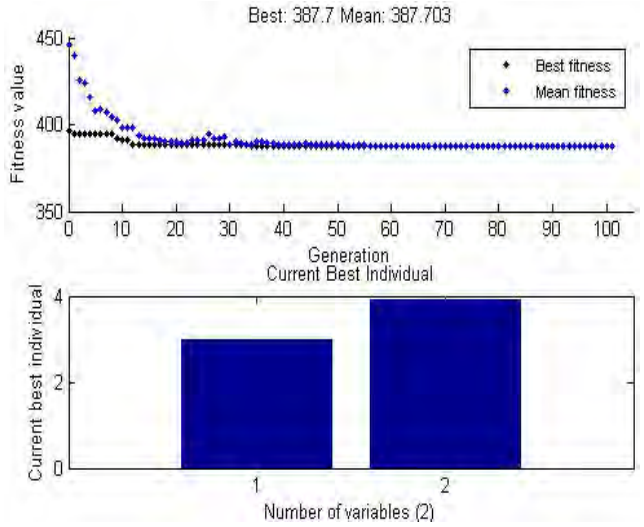

FIGURE 15. The result when the initial value is [π; 5].

The optimal value is obtained at the same time on this basis of θ and l_0. In order to solve the problem of optimal value of objective function, there are many optimization algorithms such as GA algorithm, PSO algorithm and so on. We use genetic algorithm to optimize the total power of the EHPM, as shown in Fig. 11. POS algorithm calculation result is shown in Fig. 12. The convergence speed of PSO algorithm is slower than that of GA algorithm. Particle swarm optimization algorithm is easy to fall into local optimal solution. So it is necessary to simulate several times in order to get reasonable results in this paper. In terms of convergence, GA is a more mature convergence analysis method, and can estimate the convergence rate. Therefore, the GA is used to optimize. The values of the tuning parameters of the GA are shown in Table 6.

According to Fig. 7, the optimal solution is probably not unique. The initial value of the variable largely determines its convergence range. Therefore, in the use of GA for calculation, a different initial value of variable should be chosen to observe whether the results change. Set $r_1 = 1.061$m, $\alpha = 120°$. And the boundary conditions of optimization variable is $\begin{bmatrix} 2.525 & 0 \end{bmatrix} \leq X \leq \begin{bmatrix} 3 & 2\pi \end{bmatrix}$, $X = \begin{bmatrix} l_0 & \theta \end{bmatrix}$. The results are shown in Fig. 13 when the initial value range [0; 1] is selected. The data is shown in Table 7. According to Table 7, the best individual is $l_0 = 3$m, $\theta = 45°$. And the best degree of adaptation is 387.7kW. The results are shown in Fig. 14 when the initial value range $[1; \pi]$ is selected. The data is shown in Table 8. According to Table 8, the best individual is $l_0 = 3$m, $\theta = 135°$. And the best degree of adaptation is 387.7kW. The results are shown in Fig. 15 when the initial value range $[\pi; 5]$ is selected. The data is shown in Table 9. According to Table 9, the best individual is $l_0 = 3$m, $\theta = 225°$. And the best degree of adaptation is 387.7kW. The results are shown in Fig. 16 when the initial value range

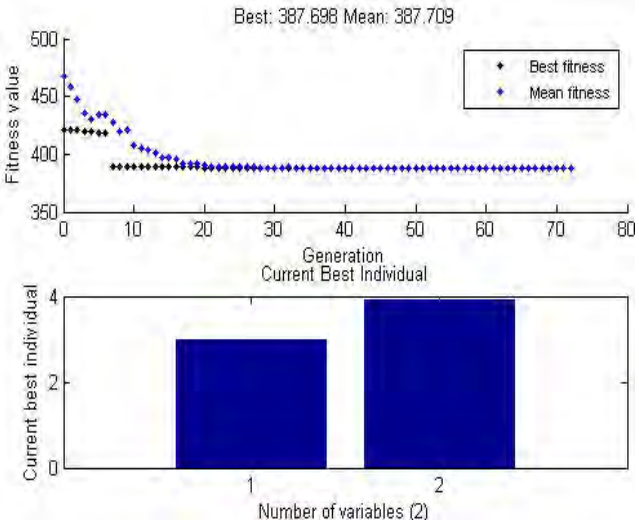

FIGURE 16. The result when the initial value is [5; 2π].

TABLE 7. The result when the initial value is [0; 1].

Decision variables	Unit	Value
Initial value	rad	[0;1]
Constraints	Unit	Value
r_1	m	1.061
α	°	120
l_0	m	[2.525;3]
θ	rad	$[0;2\pi]$
Objectives	Unit	Value
l_0	m	3
θ	°	45
P	kW	387.7

$[5; 2\pi]$ is selected. The data is shown in Table 10. According to Table 10, the best individual is $l_0 = 3$m, $\theta = 315°$. And the best degree of adaptation is 387.7kW. Assume $r_1 = 1.061$m, $\alpha = 120°$. And the boundary conditions of optimization variable is $[2.525 \quad 0] \leq X \leq [3 \quad 2\pi]$. Though we get different results by running multiple times when the initial value range $[0; 2\pi]$ is selected. They are one of the four results described above. It can be seen that the optimal solution is more than one in this section.

Hence, under the hypothesis condition and without considering the mechanical interference, the minimum total power of EHPM satisfies the conditions shown in Table 11.

V. ANALYSIS OF THE RESULTS OF OPTIMAL DESIGN

In the case of ensuring $x = [3\ 0.785]$, a different space occupied structure can be obtained by changing the position of the upper hinge point, which is shown in Fig. 17.

TABLE 8. The result when the initial value is [1; π].

Decision variables	Unit	Value
Initial value `	rad	$[1;\pi]$
Constraints	Unit	Value
r_1	m	1.061
α	°	120
l_0	m	[2.525;3]
θ	rad	$[0;2\pi]$
Objectives	Unit	Value
l_0	m	3
θ	°	45
P	kW	387.7

TABLE 9. The result when the initial value is [π; 5].

Decision variables	Unit	Value
Initial value	rad	$[\pi;5]$
Constraints	Unit	Value
r_1	m	1.061
α	°	120
l_0	m	[2.525;3]
θ	rad	$[0;2\pi]$
Objectives	Unit	Value
l_0	m	3
θ	°	225
P	kW	387.7

The parameters of the optimized structure and the classical structure are compared and analyzed as Table 12. According to Table 12, the effective area and effective working stroke of the hydraulic cylinder are decreased. The reduction of the structural parameters reduces the maximum instantaneous flow of the single cylinder by 44.6%, compared with the classical structure. The flow of the four hydraulic cylinders are essentially the same through an optimized structure. However, only two cylinders share most of the flow through the classic structure. Therefore, a smaller servo valve can be chosen. And the hydraulic springs of these two structures are substantially equal in stiffness.

TABLE 10. The result when the initial value is [5; 2π].

Decision variables	Unit	Value
Initial value	rad	$[5;2\pi]$
Constraints	Unit	Value
r_1	m	1.061
α	°	120
l_0	m	$[2.525;3]$
θ	rad	$[0;2\pi]$
Objectives	Unit	Value
l_0	m	3
θ	°	315
P	kW	387.7

TABLE 11. Conditions for the minimum total power of a hydraulic transmission system.

Decision variables	Unit	Value
	rad	$\frac{2k+1}{4}\pi(k=0,1,2,3)$
l_0	m	the maximum value under the allowable condition
Constraints	Unit	Value
r_1	m	meet the platform size requirements
α	rad	$\alpha \neq \theta$
Objectives	Unit	Value
P	kW	387.7

Fig. 18 is a fixed attitude work space under the optimized structure. Because the kinematic index of the mechanism is aimed at single degree of freedom, the attitude angle of the platform is $\phi = 0$. It can be drawn that the platform can realize the movement range of single axis ± 0.40m. In order to verify that the optimized structure can meet the requirements of the kinematic index of the platform, the fixed attitude workspace of the classical structure is shown in Fig. 19. The workspace of classical structure in a large part is a composite motion workspace that is not needed, which creates waste. It can be seen that the optimized structure is reasonable from the point of view of fixed attitude work space.

With r_1, α, θ fixed but only increasing the length of l_0 to 3.2m, a new work space is obtained and shown in Fig. 20. Comparing Fig. 20 to Fig. 18, it can be known that the work space of the optimized structure can be enlarged by increasing the length of l_0. Besides, the increase of l_0 means the decrease of total power according to Fig. 9.

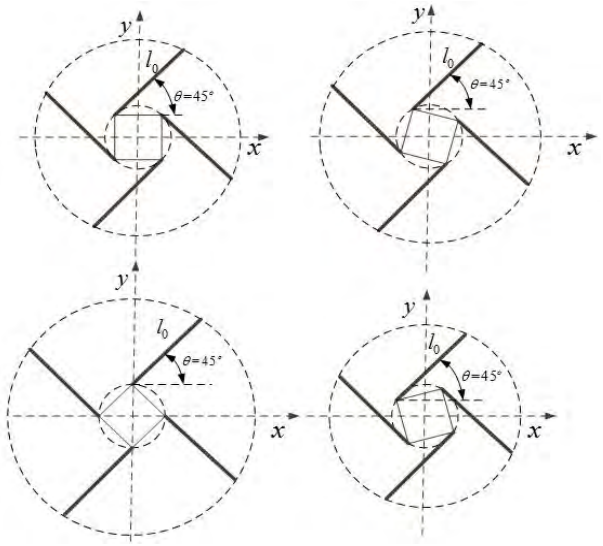

FIGURE 17. Several typical optimization structures.

TABLE 12. Structural Parameters and Classical Structural Parameters.

Contrast items	Optimized structure	Classical structure	Parameter change
Effective area of hydraulic cylinder(cm2)	10.0	14.3	Reduced
Effective working stroke of hydraulic cylinder(m)	0.5624	0.787	Reduced
Total power of hydraulic drive system(kW)	387.7	432.8	Reduced by 10.30%
Single cylinder maximum flow(L/min)	384.3	693.9	Reduced by 44.6%
Hydraulic spring stiffness(N/m)	3.98×106	3.90×106	Slightly increased
The average total flow of the system(L/min)	972.4	1062.5	Reduced by 8.49%

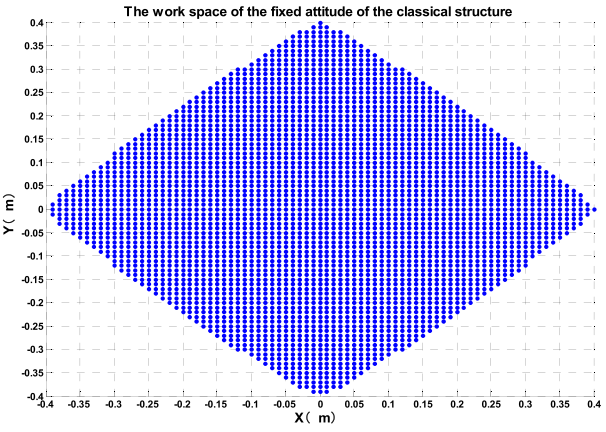

FIGURE 18. The work space of the fixed attitude of the optimized structure with $l_0 = 3$.

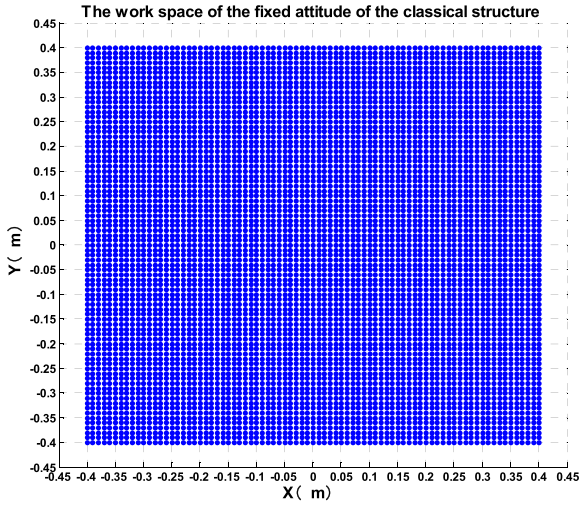

FIGURE 19. The work space of the fixed attitude of the classical structure.

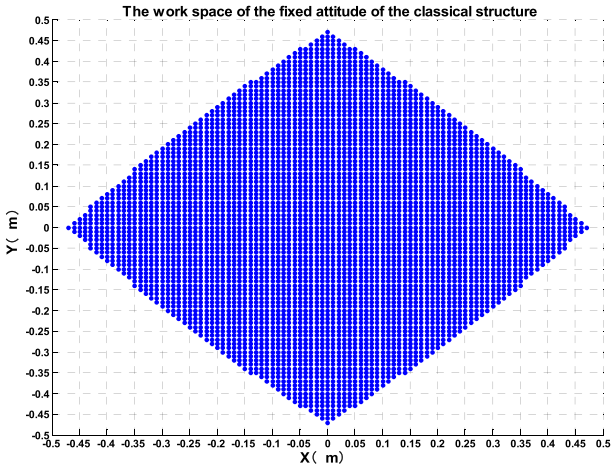

FIGURE 20. The work space of the fixed attitude of the optimized structure with increasing the length of l_0 to 3.2m.

VI. CONCLUSION

Aiming at the energy consumption of EHPM, this paper presents a new structural optimization method by changing the arrangement of the planar redundant actuator. The key of this optimization method is to identify structural variables that have an impact on total power and use GA to optimize the total power objective function with multiple structural variables. The optimal solution is obtained as $\theta = \frac{2k+1}{4}\pi$ $(k = 0, 1, 2, 3)$, $\alpha \neq \theta$. l_0 takes the maximum value under the allowable condition. r_1 needs to meet the requirements of the platform. Compared with the classic structure, the effective area and working stroke of the hydraulic cylinder are reduced by 30% and 28.5%, respectively. The four hydraulic cylinders share roughly the same flow by the optimized structure. However, only two cylinders share most of the flow by the classic structure. The maximum instantaneous flow of the single hydraulic cylinder is significantly reduced by 44.6%. Therefore, the total power of EHPM drops from 432.8kW to 387.7kW. The component selecting of hydraulic cylinder and servo valve can be smaller and the cost of which can be reduced. The structural optimization method proposed in this paper can not only apply to EHPM, but also to other electro-hydraulic servo driving parallel mechanism.

REFERENCES

[1] J. Yao, D. Di, G. Jiang, S. Gao, and H. Yan, "Real-time acceleration harmonics estimation for an electro-hydraulic servo shaking table using Kalman filter with a linear model," *IEEE Trans. Control Syst. Technol.*, vol. 22, no. 2, pp. 794–800, Mar. 2014.

[2] Z. Jinsong, S. Gang, Z. Weidong, Y. Chifu, and Y. Jing, "Robust force control with a feed-forward inverse model controller for electro-hydraulic control loading systems of flight simulators," *Mechatronics*, vol. 38, pp. 42–53, Sep. 2016.

[3] J. L. Flohic, F. Paccot, N. Bouton, and H. Chanal, "Application of hybrid force/position control on parallel machine for mechanical test," *Mechatronics*, vol. 49, pp. 168–176, Feb. 2018.

[4] X. Yu and F. Iida, "Minimalistic models of an energy efficient vertical hopping robot," *IEEE Trans. Ind. Electron.*, vol. 61, no. 2, pp. 1053–1062, Feb. 2014.

[5] X. Jia, Z. Chen, A. Riedel, T. Si, W. R. Hamel, and M. Zhang, "Energy-efficient surface propulsion inspired by whirligig beetles," *IEEE Trans. Robot.*, vol. 31, no. 6, pp. 1432–1443, Dec. 2015.

[6] J. E. Pratt, B. T. Krupp, C. J. Morse, and S. H. Collins, "The Roboknee: An exoskeleton for enhancing strength and endurance during walking," in *Proc. IEEE Int. Conf. Robot. Automat.*, New Orleans, LA, USA, Apr./May 2004, pp. 2430–2435.

[7] H. Houdijk *et al.*, "O 014—Effects of balance support on energy cost of walking with a lower limb prosthesis," *Gait Posture*, vol. 65, no. 1, pp. 25–26, Sep. 2018.

[8] M. C. Özparpucu, and A. Albu-Schäffer, "Optimal control strategies for maximizing the performance of variable stiffness joints with nonlinear springs," in *Proc. 53rd IEEE Conf. Decision Control*, Los Angeles, CA, USA, Dec. 2014, pp. 1409–1416.

[9] T. Pfau, A. Spence, S. Starke, M. Ferrari, and A. Wilson, "Modern riding style improves horse racing times," *Science*, vol. 325, no. 5938, p. 289, Jul. 2009.

[10] J. Ackerman and J. Seipel, "Energy efficiency of legged robot locomotion with elastically suspended loads," *IEEE Trans. Robot.*, vol. 29, no. 2, pp. 321–330, Apr. 2013.

[11] F. Bauer, U. Römer, A. Fidlin, and W. Seemann, "Optimization of energy efficiency of walking bipedal robots by use of elastic couplings in the form of mechanical springs," *Nonlinear Dyn.*, vol. 83, no. 3, pp. 1275–1301, Feb. 2016.

[12] F. Bauer *et al.*, "Optimal elastic coupling in form of one mechanical spring to improve energy efficiency of walking bipedal robots," *Multibody Syst. Dyn.*, vol. 38, no. 3, pp. 227–262, Nov. 2016.

[13] J. Lei, F. Wang, H. Yu, T. Wang, and P. Yuan, "Energy efficiency analysis of quadruped robot with trot gait and combined cycloid foot trajectory," *Chin. J. Mech. Eng.*, vol. 27, no. 1, pp. 138–145, Jan. 2014.

[14] A. G. Gonzalez-Rodriguez, A. Gonzalez-Rodriguez, and F. Castillo-Garcia, "Improving the energy efficiency and speed of walking robots," *Mechatronics*, vol. 24, no. 5, pp. 476–488, Aug. 2014.

[15] D. Sanz-Merodio, E. Garcia, and P. Gonzalez-de-Santos, "Analyzing energy-efficient configurations in hexapod robots for demining applications," *Ind. Robot Int. J.*, vol. 39, no. 4, pp. 357–364, 2012.

[16] V. P. Phan, N. S. Goo, K.-J. Yoon, and D.-S. Hwang, "Lookup table control method for vibration suppression of a flexible manipulator with optimization of the minimum settling time and energy consumption," *Asian J. Control*, vol. 14, no. 3, pp. 693–706, May 2012.

[17] B. Jin, C. Chen, and W. Li, "Power consumption optimization for a hexapod walking robot," *J. Intell. Robotic Syst.*, vol. 71, no. 2, pp. 195–209, Aug. 2013.

[18] J. Yao and W. Deng, "Active disturbance rejection adaptive control of hydraulic servo systems," *IEEE Trans. Ind. Electron.*, vol. 64, no. 10, pp. 8023–8032, Oct. 2017.

[19] J. Yao, W. Deng, and W. Sun, "Precision motion control for electro-hydraulic servo systems with noise alleviation: A desired compensation adaptive approach," *IEEE/ASME Trans. Mechatron.*, vol. 22, no. 4, pp. 1859–1868, Aug. 2017.

[20] Z. Yao, J. Yao, and W. Sun, "Adaptive rise control of hydraulic systems with multilayer neural-networks," *IEEE Trans. Ind. Electron.*, to be published.
[21] T. Sun, D. Liang, and Y. Song, "Singular-perturbation-based nonlinear hybrid control of redundant parallel robot," *IEEE Trans. Ind. Electron.*, vol. 65, no. 4, pp. 3326–3336, Apr. 2018.
[22] F. Procházka, M. Valášek, and Z. Šika, "Robust sliding mode control of redundantly actuated parallel mechanisms with respect to geometric imperfections," *Multibody Syst. Dyn.*, vol. 36, no. 3, pp. 221–236, Mar. 2016.
[23] J. Yao, G. Yang, and Z. Jiao, "High dynamic feedback linearization control of hydraulic actuators with backstepping," *Proc. Inst. Mech. Eng., I, J. Syst. Control Eng.*, vol. 229, no. 8, pp. 728–737, Sep. 2015.
[24] L. Pugi, M. Pagliai, A. Nocentini, G. Lutzemberger, and A. Pretto, "Design of a hydraulic servo-actuation fed by a regenerative braking system," *Appl. Energy*, vol. 187, pp. 96–115, Feb. 2017.
[25] W. Latas and J. Stojek, "A new type of hydrokinetic accumulator and its simulation in hydraulic lift with energy recovery system," *Energy*, vol. 153, pp. 836–848, Jun. 2018.
[26] L. Lu and B. Yao, "Energy-saving adaptive robust control of a hydraulic manipulator using five cartridge valves with an accumulator," *IEEE Trans. Ind. Electron.*, vol. 61, no. 12, pp. 7046–7054, Dec. 2014.
[27] S. Braune, S. Liu, and P. Mercorelli, "Design and control of an electromagnetic valve actuator," in *Proc. IEEE Int. Conf. Control Appl.*, Munich, Germany, Oct. 2006, pp. 1657–1662.
[28] A. E. K. Mohammad, N. Uchiyama, and S. Sano, "Reduction of electrical energy consumed by feed-drive systems using sliding-mode control with a nonlinear sliding surface," *IEEE Trans. Ind. Electron.*, vol. 61, no. 6, pp. 2875–2882, Jun. 2014.
[29] N. Uchiyama, Y. Ogawa, A. E. Khalick M, and S. Sano, "Energy saving in five-axis machine tools using synchronous and contouring control and verification by machining experiment," *IEEE Trans. Ind. Electron.*, vol. 62, no. 9, pp. 5608–5618, Sep. 2015.
[30] H. Kim and B. K. Kim, "Online minimum-energy trajectory planning and control on a straight-line path for three-wheeled omnidirectional mobile robots," *IEEE Trans. Ind. Electron.*, vol. 61, no. 9, pp. 4771–4779, Sep. 2014.
[31] J. Wu, B. Zhang, and L. Wang, "Optimum design and performance comparison of a redundantly actuated solar tracker and its nonredundant counterpart," *Sol. Energy*, vol. 127, pp. 36–47, Apr. 2016.
[32] B. Yao, F. Bu, J. Reedy, and G. T.-C. Chiu, "Adaptive robust motion control of single-rod hydraulic actuators: Theory and experiments," *IEEE/ASME Trans. Mechatron.*, vol. 5, no. 1, pp. 79–91, Mar. 2000.
[33] H. J. Bidgoly, A. Parsa, M. J. Yazdanpanah, and M. N. Ahmadabadi, "Benefiting from kinematic redundancy alongside mono–and biarticular parallel compliances for energy efficiency in cyclic tasks," *IEEE Trans. Robot.*, vol. 33, no. 5, pp. 1088–1102, Oct. 2017.
[34] M. Plooij, M. Wisse, and H. Vallery, "Reducing the energy consumption of robots using the bidirectional clutched parallel elastic actuator," *IEEE Trans. Robot.*, vol. 32, no. 6, pp. 1512–1523, Dec. 2016.
[35] A. Tuncer, and M. Yildirim, "Dynamic path planning of mobile robots with improved genetic algorithm," *Comput. Elect. Eng.*, vol. 38, no. 6, pp. 1564–1572, Nov. 2012.
[36] J. Lee, B.-Y. Kang, and D.-W. Kim, "Fast genetic algorithm for robot path planning," *Electron. Lett.*, vol. 49, no. 23, pp. 1449–1451, Nov. 2013.
[37] Y. Wang, Y. Zhao, S. A. Bortoff, and K. Ueda, "A real-time energy-optimal trajectory generation method for a servomotor system," *IEEE Trans. Ind. Electron.*, vol. 62, no. 2, pp. 1175–1188, Feb. 2015.
[38] P. Mercorelli, "Combining flatness based feedforward action with a fractional PI regulator to control the intake valve engine," in *Proc. 18th Int. Carpathian Control Conf. (ICCC)*, Sinaia, Romania, May 2017, pp. 456–461.

JINSONG ZHAO was born in Hebei, China, in 1983. He received the B.S. degree from Northeastern University, Liaoning, China, in 2006, and the M.S. and Ph.D. degrees in mechanical and electrical engineering from the Harbin Institute of Technology, Harbin, China, in 2008 and 2013, respectively.

He is currently a Lecturer with the Mechanical Engineering Department, Yanshan University. His research interests include series and parallel robotics, robotic design and control application, electrohydraulic servo-control technology, robotics, and rehabilitation.

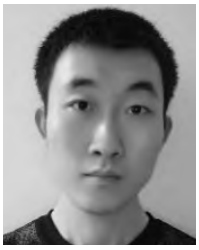

TAO YANG was born in Heilongjiang, China, in 1995. He received the B.S. degree in mechanical engineering from Yanshan University, Qinhuangdao, Hebei, China, in 2017, where he is currently pursuing the M.S. degree in mechanical engineering.

His areas of research include series robotics, robotic control application, and electrohydraulic servo-control technology.

ZHILEI MA was born in Hebei, China, in 1993. He received the B.S. degree in mechanical engineering from Yanshan University, Qinhuangdao, Hebei, in 2017, where he is currently pursuing the M.S. degree in mechanical engineering.

His areas of research include series robotics, robotic control application, and electrohydraulic servo-control technology.

CHIFU YANG was born in Hubei, China, in 1982. He received the B.S. degree in traffic engineering from the Harbin Institute of Technology, Weihai, China, in 2005, and the M.S. and Ph.D. degrees in mechanical and electrical engineering from the Harbin Institute of Technology, Harbin, China, in 2007 and 2012, respectively.

He is currently a Lecturer with the Department of Mechatronics Engineering, Harbin Institute of Technology. His current research interests include parallel robotics, robotic design and control application, electrohydraulic servo-control technology, cable-driven technology, robotics, and rehabilitation.

Dr. Yang is a member of the Editorial Board of *Advances and Applications in Mechanical Engineering and Technology*, the *International Journal of Control Engineering*, and *Technology and Science and Technology Innovation Herald*.

ZHIPENG WANG was born in Hebei, China, in 1993. He received the B.S. degree in mechanical engineering from Yanshan University, Qinhuangdao, Hebei, in 2016, where he is currently pursuing the M.S. degree in mechanical engineering.

His areas of research include parallel robotics, robotic control application, and electrohydraulic servo-control technology.

CHUNFA WANG was born in Hebei, China, in 1993. He received the B.S. degree in mechanical engineering from Yanshan University, Qinhuangdao, Hebei, in 2016, where he is currently pursuing the M.S. degree in mechanical engineering.

His areas of research include parallel robotics, robotic control application, and electrohydraulic servo-control technology.